ACS APPLIED MATERIALS & INTERFACES

www.acsami.org

Research Article

Control of Charge Carrier Relaxation at the Au/WSe_2 Interface by Ti and TiO_2 Adhesion Layers: Ab Initio Quantum Dynamics

Teng-Fei Lu, Sraddha Agrawal, Marina Tokina, Weibin Chu, Daniel Hirt, Patrick E. Hopkins, and Oleg V. Prezhdo*

Cite This: *ACS Appl. Mater. Interfaces* 2022, 14, 57197−57205

Read Online

ACCESS | Metrics & More | Article Recommendations | Supporting Information

ABSTRACT: Phonon-mediated charge relaxation plays a vital role in controlling thermal transport across an interface for efficient functioning of two-dimensional (2D) nanostructured devices. Using a combination of nonadiabatic molecular dynamics with real-time time-dependent density functional theory, we demonstrate a strong influence of adhesion layers at the Au/WSe_2 interface on nonequilibrium charge relaxation, rationalizing recent ultrafast time-resolved experiments. Ti oxide layers (TiO_x) create a barrier to the interaction between Au and WSe_2 and extend hot carrier lifetimes, creating benefits for photovoltaic and photocatalytic applications. In contrast, a metallic Ti layer accelerates the energy flow, as needed for efficient heat dissipation in electronic devices. The interaction of metallic Ti with WSe_2 causes W−Se bond scissoring and pins the Fermi level. The Ti adhesion layer enhances the electron−phonon coupling due to an increased density of states and the light mass of the Ti atom. The conclusions are robust to presence of typical point defects. The atomic-scale ab initio analysis of carrier relaxation at the interfaces advances our knowledge in fabricating nanodevices with optimized electronic and thermal properties.

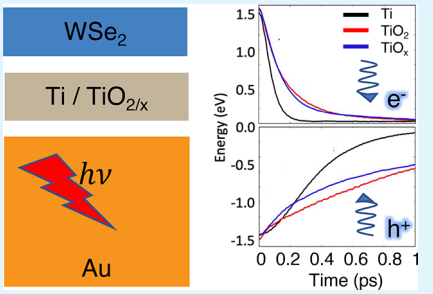

KEYWORDS: *nonadiabatic molecular dynamics, charge carrier relaxation, time-dependent density functional theory, Au/WSe_2 interface, adhesion layer*

INTRODUCTION

Scientific understanding of thermal transport in nanoscale systems is crucial to tackling the problem of thermal management in various applications including optoelectronics and thermoelectrics.[1−4] Development of improved electronic and photoelectric devices requires high thermal conductivity materials that can dissipate heat faster.[1] On the other hand, materials with low thermal conductivity and low electrical resistance are important for applications in thermoelectric devices converting waste heat into useful electrical energy.[5−7] Understanding phonon transport and thermal conductivities in materials is extremely important for the engineering of novel nanodevices.

As a relatively new class of layered materials, 2D transition metal dichalcogenides (TMDs) have attracted significant attention in the last few decades due to their semiconducting characteristics, excellent chemical stability, and tunable mechanical and physical properties.[8−10] They find applications in a wide variety of fields: A relatively high electrical conductivity and a relatively low thermal conductivity make TMDs promising materials for next-generation high-performance thermoelectric devices.[11−13] Monolayer WSe_2, due to its heavy atom mass and low Debye frequency, has been found to have ultralow thermal conductivity, even lower than that in MoS_2.[14,15] The observations and understanding derived from the studies of the corresponding bulk nanostructured materials have stimulated further research on thermoelectric energy conversion.[16]

The presence of interfaces has grown more ubiquitous in the fabrication of nanoelectronics owing to rapid miniaturization of device dimensions.[17,18] Energy exchange between phonons and respective charge carriers in each material comprising the interface is involved in the interfacial energy transfer.[19−25] Consequently, several theoretical models have also been developed to mimic ultrafast pulsed laser experiments that are widely used to study nonequilibrium processes involving such electron-vibrational energy exchange.[25−30] Thermal transport across two metal interfaces is controlled by electrons near the Fermi energy, yielding thermal boundary conductance values that are far higher than those across metal/nonmetal interfaces.[31] The overall thermal resistance in nanoscale devices is dominated by scattering of phonons at boundaries rather than the intrinsic thermal resistance of a material.[32] Higher electronic conductivity at the interface is more important than that of the adhesion layer for faster energy

Received: October 19, 2022
Accepted: December 5, 2022
Published: December 14, 2022

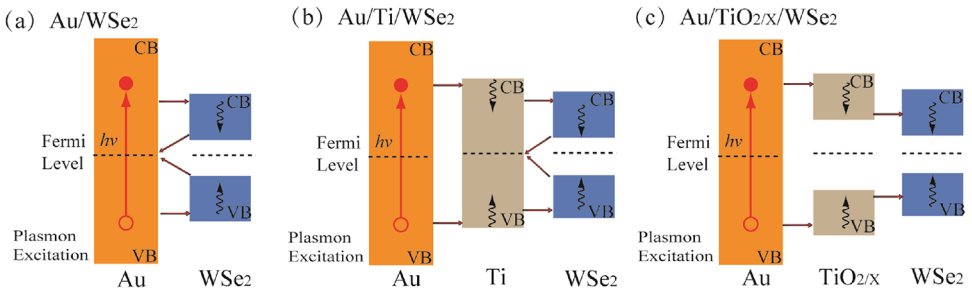

Figure 1. Schematic of the photoinduced hot charge carrier relaxation processes from the initial high energy state to the Fermi level in the presence of different adhesion layers at the Au/WSe_2 interface. (a) Photogenerated in Au, hot charge carriers transfer from Au to WSe_2, in which they relax faster by coupling to the lighter Se atoms and then transfer back to Au and recombine. (b) The photogenerated charges travel from Au, through Ti to WSe_2. They relax fast by coupling to lighter Ti and Se atoms and recombine inside Ti. (c) Generated with sufficiently high energy, charge carriers travel through TiO_2 to WSe_2, in which they relax to the band edges and cannot travel back to Au, if TiO_2 is sufficiently thick and creates a tunneling barrier.

transport across the interface, provided the adhesion layer is sufficiently narrow. At the same time, for faster energy transport within a material (or adhesion layer, here), higher electronic conductivity would be beneficial. It is, therefore, critical to focus on unraveling the fundamental thermal transport mechanisms at interfaces for building high-performance devices. This is especially true for TMD materials, which have been shown to exhibit record setting high thermal resistance at interfaces[33] and novel electron and phonon interfacial transport processes that have led to emergent energy conversion devices.[34]

In the past, significant efforts have been made to tune the electrical and thermal boundary resistance for optimizing the device performance in desired applications.[35−38] Several experimental and theoretical studies have shown a decrease in electrical contact resistance by deposition of thin oxide layers at the metal−semiconductor interface.[39−41] Conversely, a substantial increase in thermal boundary resistance is seen due to the presence of native oxides at the interface.[18,21,42,43] Stronger chemical and electronic interactions across the interface are responsible for higher thermal boundary conductance, as observed in a theoretical study.[18,44] Recently, the experimental work by Freedy et al. has demonstrated ∼20% lower thermal boundary conductance in Au/TiO_x/MoS_2 as compared to Au/Ti/MoS_2 and Au/Ti/TiO_x/MoS_2 due to the different interfaces with the top Au contact.[32] Further, reduced thermal boundary conductance and higher electrical resistance are observed in Au−TiO_x−WSe_2−HOPG (highly oriented pyrolytic graphite) interfaces due to lack of reactivity of the interfacial oxide with the semiconductor layer than in the corresponding pure metal Ti interlayer.[45] These observations indicate diminished thermal transport in the presence of an oxide layer and, thus, lay an emphasis on the dependence of boundary resistance on interface chemistry of related materials. To advance our understanding of this interfacial behavior, a detailed theoretical description explaining the differences in energy transport at various interfaces is required. The description should account for the atomistic details of the interfacial interactions and consider the far-from-equilibrium nature of the energy exchange processes.

In the present work, we report a time−domain ab initio analysis of phonon-induced nonradiative charge carrier relaxation in the presence of pure metallic Ti and TiO_x oxide layers at the Au/WSe_2 interface. The simulations are performed using a state-of-the-art nonadiabatic molecular dynamics (NAMD) approach formulated within the framework of real-time time-dependent density functional theory (TDDFT) in the Kohn Sham (KS) representation. The methodology used mimics the ultrafast pump-probe optical experiments of charge carrier dynamics and provides an atomistic insight into the nonequilibrium nature of the charge scattering and relaxation processes at interfaces. A schematic of the relaxation of hot charge carriers from the initial high energy state to the Fermi level in the presence of different interfacial layers is shown in Figure 1. The charge relaxation is significantly slower in the presence of Ti oxide layers at the metal/semiconductor interface than in the presence of a metallic Ti adhesion layer, as rationalized by differences in the interfacial chemical interactions, local densities of states (DOSs), energy level alignment, participation of particular phonon modes, and presence of atomic defects. The study indicates that metallic adhesion layers are beneficial for electronic devices, while oxide layers are more appropriate for solar energy applications.

COMPUTATIONAL DETAILS

The simulations are performed using a mixed quantum-classical technique.[46] Here, electronic evolution is modeled using real-time TDDFT[47] while classical MD describes the nuclear motions. The electron−nuclear interactions in charge relaxation processes are investigated using fewest-switches surface hopping (FSSH),[48,49] one of the most common NAMD methods, as implemented in the PYXAID code under the classical path approximation (CPA).[50,51] The methodology has been successfully applied to study excited-state dynamics in various nanoscale systems.[52−60] A more detailed description of the time−domain DFT and NAMD methods used can be found in the Supporting Information.

The electronic structure calculations and adiabatic MD are carried out using the Vienna Ab initio Simulation Package (VASP).[61] The generalized gradient approximation (GGA) with the Perdew−Burke−Ernzerhof (PBE)[62] exchange−correlation functional and the projector-augmented wave (PAW)[63] pseudopotentials are used. The van der Waals (vdW) interactions at the interface are described by the Grimme DFT-D3 method.[64] VDW-D2/D3 and opt-B86/88b-DF are routinely applied to account for van der Waals interactions in bilayers and multilayers. A comparison of VDW-D2 and VDW-D3 shows that PBE-D3 performs better than PBE-D2 in materials such as MoS_2.[65] In some other cases, the VDW-D2 method provides the strongest dispersion interaction, whereas optB86b-vdW gives the weakest.[66]

https://doi.org/10.1021/acsami.2c18793
ACS Appl. Mater. Interfaces 2022, 14, 57197−57205

Different vdW corrections would only slightly affect the quantitative interlayer distances and interactions reported here. The qualitative trends and NAMD results and conclusions drawn in this work would remain the same. The energy cutoff for the plane-wave basis is set to 400 eV. A 5 × 5 × 1 Monkhorst−Pack k-point mesh is used for geometry relaxation and DOS and MD calculations. To model the Au/Ti/WSe_2 system, a supercell of the Au (111) surface with five layers containing forty Au atoms, a WSe2 monolayer with six W and twelve Se atoms, and a single Ti(001) layer with eight atoms sandwiched between Au and WSe_2 is constructed using VESTA.[67] In the Au/TiO_2/WSe_2 system, four Ti and eight O atoms are used while in Au/TiO_x/WSe_2, one O of TiO_2 is switched with a Se of WSe_2, representing a common defect.[45] A vacuum layer of 20 Å is introduced perpendicular to the surface to eliminate interactions between periodic images of the slabs.

The systems are optimized and then heated to 300 K using repeated velocity rescaling to obtain thermally equilibrated structures. Then, 4 ps adiabatic MD trajectories are generated in the microcanonical ensemble with a 1 fs time step and are used for the NA coupling (NAC) calculations.[68,69] Five hundred geometries selected from the adiabatic MD trajectory are used as initial conditions for NAMD, and 1000 stochastic realizations are sampled for each initial condition. The 4 ps trajectories are repeated twice to obtain longer NAMD trajectories.

The employed approach has several advantages over the more traditional techniques, such as the quantum transport calculations.[70−72] Real-time TDDFT makes no assumptions that the evolution is determined by a particular form of kinetics, e.g., exponential, which allows one to determine a transport rate. The calculated results show that the dynamics are neither exponential nor Gaussian. The evolution is obtained by solving the time-dependent Schrodinger equation in the KS form, including memory effects and electron-vibrational coupling that depends on evolving atomic geometry. The calculations do not assume that the electron-vibrational coupling is weak. The weak coupling assumption is typically used to obtain rates for the quantum transport calculations. The calculated coupling shows significant energy dependence. The method does not assume that vibrations are harmonic. This is particularly important for systems with surfaces, interfaces, and defects, which exhibit anharmonic motions dynamics. Anharmonicity relaxes electron−phonon coupling selection rules and allows more vibrational modes to couple to the electronic subsystem.

RESULTS AND DISCUSSION

The optimized structures of Au/Ti/ WSe_2, Au/TiO_2/WSe_2, and Au/TiO_x/WSe_2 are illustrated in Figure 2. The three structures differ in the interlayer present between Au slab and WSe_2 monolayer. We use two types of titanium oxide layers in two different structures: TiO_2 and TiO_x. TiO_2 is the most stable and common form of stoichiometric titanium oxide, in which Ti is in the +4 oxidation state. TiO_x is a sub-stoichiometric interlayer with x slightly less than 2. Such composition is encountered commonly in experiments.[45] In our study, the sub-stoichiometric TiO_x is modeled by introduction of the common structural defect, in which one oxygen of TiO_2 is interchanged with a Se of WSe_2, resulting in the formation of a W−O bond and a Ti−Se bond. The nearest Au−Ti and Ti−WSe_2 distance in Au/Ti/WSe_2 is smaller than

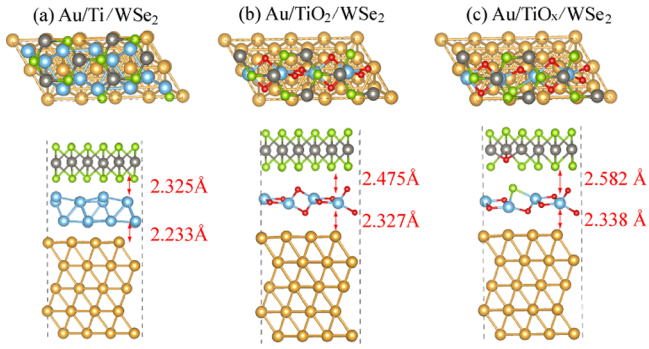

Figure 2. Top and side views of the simulation cells showing the optimized structures of (a) Au/Ti/WSe_2, (b) Au/TiO_2/WSe_2, and (c) Au/TiO_x/WSe_2. To make the TiO_x system, one O of TiO_2 is switched with a Se of WSe_2 representing a typical defect. The numbers on the right side of the structures indicate the distances between the two adhesion layers. The Ti layer has similar thickness compared to the TiO_2 and TiO_x layers. Ti provides stronger adhesion than TiO_2.

the interlayer distances of the other two systems with interfacial oxide layers, indicating that the interlayer chemical interactions is the strongest in the system with metallic Ti. This strong interaction of the pure Ti layer in Au/Ti/WSe_2 with WSe_2 leads to scissoring of W−Se bonds and formation of metallic W. The trend of the interlayer distances remains the same in both the optimized structures and the ambient temperature. The values of adjacent layer distances averaged over the entire trajectories at 300 K are presented in Table S1 of the Supporting Information. The dependence of interfacial interaction strength on the type of adhesion layer influences the electronic structure of the systems and in turn affects the electron−phonon energy transfer and charge carrier relaxation.

To understand the dependence of the electronic structure on the nature of interlayer present in the systems studied, we have shown the projected DOS (PDOS) along with the charge densities at the Fermi level in Figure 3. There is no band gap in the DOS of Au owing to its fully metallic nature in all the three systems. It is interesting to note that the appearance of metallic W due to the interaction of elemental Ti and WSe_2 and W−Se bond scissoring in Au/Ti/WSe_2 results in an almost negligible band gap of WSe_2, characteristic of a metallic system. The strong Ti−Se interaction weakens the nearest W−Se covalent bonding, leading to the introduction of new electronic states in the WSe_2 band gap, resulting in Fermi-level pinning. In contrast, the presence of an interfacial oxide layer, i.e., TiO_2 or TiO_x, prevents the chemical reaction between Ti and the monolayer, keeping the structure of WSe_2 intact. In the absence of any interfacial reaction products, WSe_2 retains its intrinsic band structure with a band gap ∼1.5 eV due to no appearance of any new states, which can pin the Fermi level. Addition of the interfacial oxide layer has only a minor influence on the electronic structure of the WSe_2 layer. In particular, the band gap of WSe_2 is maintained. Further, the TiO_2 layer has a larger band gap than the WSe_2 layer[73] (Figure 1c). Therefore, if photogenerated charges enter from Au to WSe_2 through the TiO_2 layer and the TiO_2 layer is sufficiently thick, the charges relax to the WSe_2 band edges and cannot go back to Au, because TiO_2 creates a tunneling barrier, i.e., there are no states inside TiO_2 at the relevant energy to facilitate electron transport from the WSe_2 band edge to Au. This diode effect is not seen in the current simulation, because the TiO_2

https://doi.org/10.1021/acsami.2c18793
ACS Appl. Mater. Interfaces 2022, 14, 57197−57205

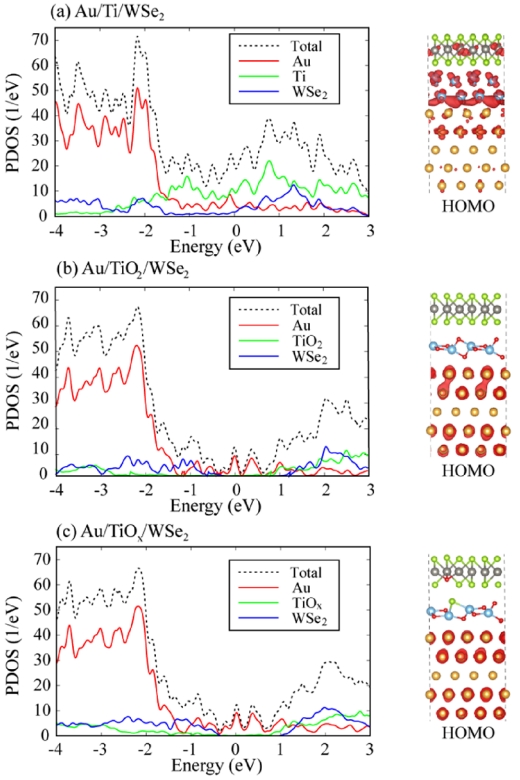

Figure 3. Projected density of states (PDOS) in the left panel and charge densities of the highest occupied molecular orbitals (HOMO) in the right panel of (a) Au/Ti/WSe_2, (b) Au/TiO_2/WSe_2, and (c) Au/TiO_x/WSe_2. The Fermi level is set to zero. Ti contributes strongly to the PDOS around the Fermi level, while TiO_2 has an energy gap. The O/Se switch defect has little influence on the PDOS and charge densities. The Fermi level charge density of the Au/Ti/WSe_2 system is delocalized over Au, Ti, and even W, while the charge densities of the other systems are localized solely on Au.

layer is too thin. These results are consistent with the experimental studies on similar systems.[32,45] The corresponding PDOS and atomic structures for a thicker interlayer (double the thickness of the original interlayer), shown in Figure S1, demonstrate similar results. The interlayer thickness comparison exhibits that the electronic properties here depend on the type of interlayer present rather than on the thickness of the middle layers used. This observation has also been reported in the previous studies.[32] Hence, further calculations were done using a single layer of Ti, TiO_2, or TiO_x, due to high computational cost of the real-time TDDFT/NAMD calculations.

The DOS at energies below −2 eV is large, and it significantly decreases above −2 eV. This asymmetry in DOS implies that the relaxation of holes deep in the valence band (VB) in the high-DOS region should be much faster as compared to both the relaxation of excited holes closer to the Fermi energy and the relaxation of electrons above the Fermi level. The PDOS for structures with oxide layers is quite similar with very minute differences; therefore, we expect similar results for the TiO_2 and TiO_x systems. In all systems, the PDOS of Au decreases drastically in the energy range between −2 and −1 eV and remains almost the same throughout the energy range shown. In Au/Ti/WSe_2, the PDOS of Ti starts increasing beyond −2 eV to higher energy states and goes above the PDOS of Au. At energies above −1.5 eV, the PDOS of a single Ti layer is higher than the PDOS of the five-layer Au slab. In the energy range of −1.55 to 1.55 eV, high PDOS of Ti and small contributions from WSe_2 around the Fermi level for the system with the metallic Ti layer will favor faster charge carrier relaxation as compared to the other two systems with the interfacial oxide layer, which have negligible PDOSs near the Fermi level. The DOS is slightly higher above 0 eV than below 0 eV. This would, thus, favor faster electron relaxation as compared to hole relaxation. For further understanding of electronic structure of the systems studied, we have also plotted the electronic band structures of all the systems in Figure S2 of the SI.

Charge densities of the HOMO, shown on the right panels of Figure 3, support the observations from the PDOS. In case of Au/Ti/WSe_2, the charge density of the HOMO shows maximum electron density localization on Ti followed by localization on W of WSe_2. This is attributed to the increased DOS of WSe_2 near the Fermi energy, resulting from Fermi-level pinning due to Ti−WSe_2 interlayer interaction and scissoring of the W−Se bonds. The localization of the charge density on Au is smaller than on Ti, which matches the smaller PDOS of Au near the Fermi level. On the other hand, for the systems with the interfacial oxide layers, the maximum charge density localizes on Au as compared to density localization on TiO_2 or WSe_2. This is again consistent with the PDOS observations where contribution of TiO_2 or WSe_2 is negligible near the Fermi energy due to a weak interlayer interaction in these two systems.

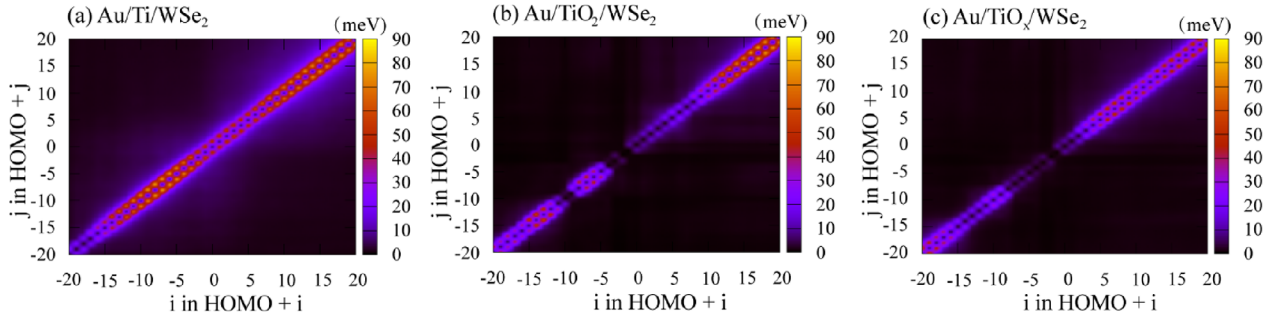

Figure 4. Visualization of the averaged absolute nonadiabatic couplings (NACs) between states labeled by orbital indices for (a) Au/Ti/WSe_2, (b) Au/TiO_2/WSe_2, and (c) Au/TiO_x/WSe_2. The orbitals cover the energy range from about −1.5 eV to about 1.5 eV relative to the Fermi level, corresponding to the energy range of the quantum dynamics calculations (Figure 5). The NACs are largest near the diagonal, indicating that the electron−phonon relaxation occurs by frequent transitions between nearby states. In the presence of Ti, the NACs are large across the whole energy range, while regions of small NACs are seen in the other two systems.

https://doi.org/10.1021/acsami.2c18793
ACS Appl. Mater. Interfaces 2022, 14, 57197−57205

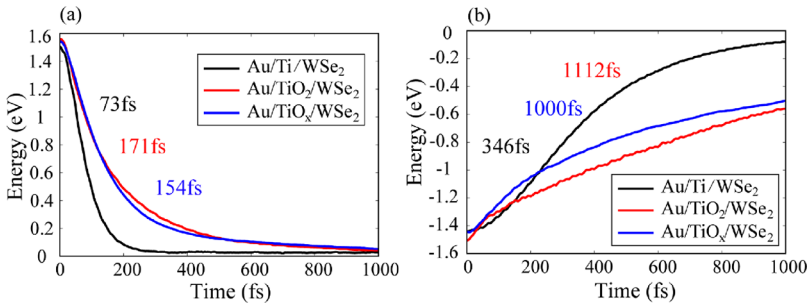

Figure 5. Evolution of the (a) electron and (b) hole energy starting from initial states at 1.55 eV and −1.55 eV, respectively. Electrons decay faster than holes because of the larger NAC above vs below the Fermi energy (Figure 4), correlated with the larger contribution of Ti and TiO_2 to the PDOS at 1.55 vs −1.55 eV (Figure 3). Ti and O are the lightest atoms in the systems, generating the strongest electron−phonon coupling. Both electrons and holes relax two to three times faster in the presence of Ti vs TiO_2 because of the large contribution of Ti to the PDOS in the −1.55 to 1.55 eV energy range (Figure 3). The O/Se switch defect accelerates the relaxation by about 10%.

Both elastic and inelastic electron−phonon scatterings are known to influence the charge carrier dynamics. Elastic scattering leads to loss of quantum coherence in the electronic subsystem, whereas inelastic scattering dissipates electronic energy to heat through nonradiative relaxation pathways. Elastic scattering, reflected by the pure-dephasing time, becomes generally important for study of processes occurring across large energy gaps,[74] such as charge recombination in semiconductors.[46,75] On the other hand, elastic scattering is less important for hot carrier relaxation that takes place over dense manifold of states. Such intraband relaxation is governed by inelastic electron−phonon coupling, which is characterized by the NAC that serves as the primary focus of the analysis here. The NAC strength depends on the electron−phonon coupling matrix element and the nuclear velocity, as shown in eq S5 given in the Supporting Information. Figure 4 visualizes the average NAC values for all pairs of orbitals in the relevant energy window around the Fermi level. The NAC is maximum for pairs of nearest states and is much smaller for all other pairs of states. This fact indicates that NA transitions between adjacent states close in energy contribute most to the hot carrier relaxation pathway.

Figure 4 illustrates consistently larger NAC values for Au/Ti/WSe_2 in the observed energy range as compared to the other two systems with interfacial oxide layers. This observation strongly correlates with the corresponding PDOS results. By introducing additional states near the Fermi level, the metallic Ti layer increases the DOS as compared to the other systems. The NAC is inversely proportional to the energy gap between the corresponding pair of states, and the larger DOS decreases the energy level spacing. In addition, the larger number of states provides more relaxation channels. Further, we also notice a higher NAC for orbitals above the Fermi level (Figure 4), which would influence the difference in electron and hole relaxation dynamics. The higher NAC above the Fermi level correlates with the more significant contribution of Ti and TiO_2 at the higher energies (Figure 3). The lightest atoms in the systems, Ti and O, create a strong NAC, since the NAC is proportional to the nuclear velocity (eq S5).

In the simulations, the electrons and holes are photoexcited to 1.55 eV above and below the Fermi level, respectively, representing a typical Ti:sapphire laser excitation. The phonon-assisted energy relaxation of the hot charge carriers from the initial high energy states to the Fermi energy is shown in Figure 5. The time constants reported in the figure are obtained by fitting the data to exponential functions, $E = E_0 \exp.(-t/\tau)$, where the E_0 initial energy can be positive or negative. Figure 5 demonstrates that both electrons and holes relax two to three times faster in Au/Ti/WSe_2 as compared to the other two systems and that the hot electron relaxation is faster than the hole relaxation in all systems. Figure S3 presents electron and hole relaxation dynamics in the Au/WSe_2 system. The relaxation in the absence of the adhesion layers is significantly slower, because the adhesion layers increase the interfacial interactions and contain light atoms, both factors enhancing the electron-vibrational interactions. It is quite remarkable that thin Ti and TiO_x adhesion layers can have such a significant influence on the hot carrier relaxation at the metal/semiconductor interface.

The difference in the relaxation times can be rationalized by considering the fact that the transition rate depends on the NAC and DOS, as represented, for instance, by Fermi's golden rule. The metallic Ti system has a higher PDOS and a larger NAC as compared to the other two systems with oxide layer, seen in Figures 3 and 4. On the other hand, the relaxation timescales for the TiO_2 and TiO_x interlayer systems are of the same order of magnitude because of similar DOS and NAC. The ab initio quantum dynamics simulation results are, thus, in alignment with the expectations based on the DOS and NAC strength. A similar reasoning holds true for explaining the difference in electron and hole relaxation timescales. The DOS and NAC in the 0 to 1.55 eV range are higher than those in the −1.55 to 0 eV range. On the one hand, the slow charge relaxation observed in the presence of the oxide interlayer can be exploited to extract hot charge carriers for various photovoltaic and photocatalytic applications.[76] On the other hand, systems containing metallic adhesion layers made of light elements provide strong benefits for electronics applications requiring rapid heat dissipation.

Interfacial defects can play an important role in the electron−phonon relaxation process. An example of an interfacial defect is shown in Figure 2c. An O atom of the TiO_2 adhesion layer and a Se atom of WSe_2 are switched. Figure 3b,c demonstrates that the defect has little influence on the overall DOS. On the other hand, Figure 5 shows that both electron and hole relaxation are accelerated by about 10%. The faster charge relaxation in the defective system is due to participation of additional vibrational modes, which are activated by the introduced disorder and symmetry breaking, as analyzed in Figure 6 below.

https://doi.org/10.1021/acsami.2c18793
ACS Appl. Mater. Interfaces 2022, 14, 57197−57205

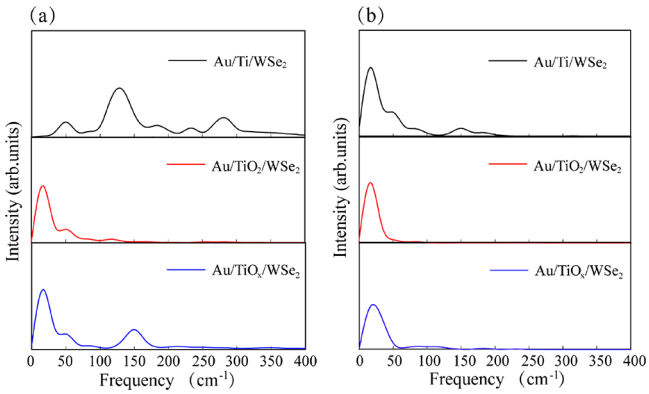

Figure 6. Phonon influence spectra for the (a) electron and (b) hole relaxations in the three investigated systems. The high frequencies arising from Ti motions dominate the spectra for electron relaxation and are present for hole relaxation in Au/Ti/WSe_2. The system Au/TiO_2/WSe_2 shows no such modes. Ti signals are seen in the Au/TiO_x/WSe_2 system containing the O/Se switch defect.

To gain more insights into the difference in the electron−phonon scattering in the three systems, we compute Fourier transforms (FT) of the autocorrelation functions of the energy gaps between the initial and final pairs of states, shown in Figure 6. The FTs, also known as phonon influence spectra, characterize the phonon modes that couple to the electronic subsystem and lead to loss of energy during the corresponding nonradiative transitions. FTs identify the vibrational frequencies that induce fluctuations of energy gaps due to movement of atoms. The amplitude of a spectral peak reflects the strength of the charge-phonon coupling corresponding to that specific frequency.

The phonon influence spectra (Figure 6) show that the prominent modes involved in the nonradiative charge relaxation have frequencies below 200 cm^{-1}, except for the electron relaxation in Au/Ti/WSe_2. Additional higher frequencies participate in electron relaxation as compared to hole relaxation in all three systems. This result supports the faster relaxation timescale observed for electrons as supposed to holes, because higher-frequency phonons generate large velocities and strengthen the NAC that is proportional to the velocity (eq S5). The intense peak below 100 cm^{-1} has been assigned to acoustic phonons of Au.[37] The higher-frequency modes arise from the lighter Ti and O atoms in the systems. The peak heights of different phonon modes suggest that the lower-frequency acoustic modes provide stronger coupling than the higher-frequency optical phonons. This is because the phase of atomic oscillation changes rapidly across the system for optical modes. In particular, the nuclear velocities of adjacent atoms have opposite signs for optical modes, and contributions of different atoms to the overall NAC cancel each other (eq S5). In comparison, nearby atoms move in the same direction during acoustic motions and their contributions to the NAC add up. Participation of multiple higher energy modes in case of the elemental Ti interlayer rationalizes the faster charge relaxation compared to the system with the oxide layers (Figure 5). Compared to the defect-free Au/TiO_2/WSe_2 system, the symmetry breaking and disorder introduced by the defect in the Au/TiO_x/WSe_2 system activates additional vibrational modes and also accelerates the charge relaxation, although to a much lesser extent than the metallic Ti adhesion layer.

CONCLUSIONS

We have performed ab initio quantum dynamics investigation of electron−phonon relaxation at the Au−WSe_2 interface containing metallic and semiconducting adhesion layers and have demonstrated a strong dependence of the rate of energy flow on the adhesion layer. The simulations have been carried out using a state-of-the-art technique developed in our group combining TDDFT and NAMD, mimicking most directly the nonequilibrium nature of the relaxation processes. The difference in the charge carrier dynamics timescales in the presence of the pure metallic adhesion layer versus the oxide layers is rationalized through various factors governing the quantum dynamics. The results obtained in this work rationalize the experimental observation that the presence of an oxide layer in the interface of Au and WSe_2 lead to a lower thermal boundary conductance, compared to a metallic adhesion layer, implying slower hot charge relaxation across the interface. The suppressed charge relaxation in the systems with the TiO_2 and TiO_x interlayers is attributed to two major factors. First, the oxide layer prevents the interaction of the WSe_2 semiconductor with the Au metal, keeping the intrinsic band gap of WSe_2 intact. In comparison, the interaction of metallic Ti with WSe_2 leads to formation of metallic W and introduces additional electronic states around the Fermi energy and causes Fermi-level pinning. Second, since Ti atoms are lighter than Au, W, and Se atoms, and pure Ti contributes electronic states near the Fermi energy, the Ti adhesion layer introduces higher-frequency phonon modes enhance electron−phonon coupling. The results are robust to introduction of typical point defects: The electron-vibrational relaxation in the system with a sub-stoichiometric TiO_x is only slightly faster than in the system with the stoichiometric TiO_2 layer. Thus, oxide layers create a barrier for the flow of charges and energy across the interface and, therefore, increase the thermal boundary resistance in optoelectronic devices. On the other hand, adhesion layers composed of light metals increase the thermal boundary conductance. The control of the interfacial energy flow by stoichiometry of the adhesion layer can be used to tune the systems for a particular application. Fast energy flow, facilitated by metallic adhesion layers, is beneficial for thermal energy dissipation in electronic devices, while slow electron-vibrational relaxation in the presence of oxide layers extends lifetimes of hot charge carriers and can be useful in photovoltaic and photocatalytic applications. The work presented here facilitates the understanding of the fundamental mechanisms underlying far-from-equilibrium phonon-mediated relaxation of hot charge carriers in multilayer systems, guiding the design of novel materials toward various optoelectronic applications.

ASSOCIATED CONTENT

Supporting Information

The Supporting Information is available free of charge at https://pubs.acs.org/doi/10.1021/acsami.2c18793.

Densities of states for the systems with thicker TiO_x layers; simulation results for Au/WSe_2; electronic band structures; interlayer distances at 300 K; description of time−domain density functional theory; and fewest-switches surface hopping (PDF)

https://doi.org/10.1021/acsami.2c18793
ACS Appl. Mater. Interfaces 2022, 14, 57197−57205

AUTHOR INFORMATION

Corresponding Author

Oleg V. Prezhdo − *Department of Chemistry and Department of Physics and Astronomy, University of Southern California, Los Angeles, California 90089, United States;* orcid.org/0000-0002-5140-7500; Email: prezhdo@usc.edu

Authors

Teng-Fei Lu − *School of Materials Science and Engineering, Dalian Jiaotong University, Dalian 116028 Liaoning Province, China*

Sraddha Agrawal − *Department of Chemistry, University of Southern California, Los Angeles, California 90089, United States*

Marina Tokina − *Department of Chemistry, University of Southern California, Los Angeles, California 90089, United States*

Weibin Chu − *Key Laboratory of Computational Physical Sciences (Ministry of Education), Institute of Computational Physical Sciences, Fudan University, Shanghai 200433, People's Republic of China;* orcid.org/0000-0001-5951-0337

Daniel Hirt − *Department of Mechanical and Aerospace Engineering, University of Virginia, Charlottesville, Virginia 22904, United States*

Patrick E. Hopkins − *Department of Mechanical and Aerospace Engineering, Department of Materials Science and Engineering, and Department of Physics, University of Virginia, Charlottesville, Virginia 22904, United States*

Complete contact information is available at: https://pubs.acs.org/10.1021/acsami.2c18793

Notes

The authors declare no competing financial interest.

ACKNOWLEDGMENTS

The research was supported by the US Department of Defense, Multidisciplinary University Research Initiative, grant no. W911NF-16-1-0406, and the Semiconductor Research Corporation, Award Number 2021-NM-3047.

REFERENCES

(1) Pop, E. Energy Dissipation and Transport in Nanoscale Devices. *Nano Res.* **2010**, *3*, 147−169.

(2) Shi, J.; Yuan, C.; Huang, H. L.; Johnson, J.; Chae, C.; Wang, S.; Hanus, R.; Kim, S.; Cheng, Z.; Hwang, J.; et al. Thermal Transport across Metal/Beta-Ga2o3 Interfaces. *ACS Appl. Mater. Interfaces* **2021**, *13*, 29083−29091.

(3) Cahill, D. G.; Braun, P. V.; Chen, G.; Clarke, D. R.; Fan, S.; Goodson, K. E.; Keblinski, P.; King, W. P.; Mahan, G. D.; Majumdar, A.; et al. Nanoscale Thermal Transport. Ii. 2003−2012. *Appl. Phys. Rev.* **2014**, *1*, 011305.

(4) Jung, S.-K.; Hwang, I.; Chang, D.; Park, K.-Y.; Kim, S. J.; Seong, W. M.; Eum, D.; Park, J.; Kim, B.; Kim, J.; et al. Nanoscale Phenomena in Lithium-Ion Batteries. *Chem. Rev.* **2020**, *120*, 6684−6737.

(5) Sledzinska, M.; Quey, R.; Mortazavi, B.; Graczykowski, B.; Placidi, M.; Saleta Reig, D.; Navarro-Urrios, D.; Alzina, F.; Colombo, L.; Roche, S.; et al. Record Low Thermal Conductivity of Polycrystalline Mos2 Films: Tuning the Thermal Conductivity by Grain Orientation. *ACS Appl. Mater. Interfaces* **2017**, *9*, 37905−37911.

(6) Yoshihama, H.; Kaneko, H. Design of Thermoelectric Materials with High Electrical Conductivity, High Seebeck Coefficient, and Low Thermal Conductivity. *Anal. Sci. Adv.* **2021**, *2*, 289−294.

(7) Finn, P. A.; Asker, C.; Wan, K.; Bilotti, E.; Fenwick, O.; Nielsen, C. B. Thermoelectric Materials: Current Status and Future Challenges. *Front. Electron. Mater.* **2021**, *1*, No. 677845.

(8) Kim, K. S.; Kim, K. H.; Kang, J. E.; Lee, J.-H.; Ji, Y. J.; Yeom, G. Y. Atomic Layer Engineering of Tmds by Modulation of Top Chalcogen Atoms: For Electrical Contact and Chemical Doping. *ACS Appl. Electron. Mater.* **2022**, *4*, 3794−3800.

(9) Kang, J.; Liu, W.; Sarkar, D.; Jena, D.; Banerjee, K. Computational Study of Metal Contacts to Monolayer Transition-Metal Dichalcogenide Semiconductors. *Phys. Rev. X* **2014**, *4*, No. 031005.

(10) Choi, W.; Kim, J.; Lee, E.; Mehta, G.; Prasad, V. Asymmetric 2d Mos2 for Scalable and High-Performance Piezoelectric Sensors. *ACS Appl. Mater. Interfaces* **2021**, *13*, 13596−13603.

(11) Zhao, Y.; Cai, Y.; Zhang, L.; Li, B.; Zhang, G.; Thong, J. T. L. Thermal Transport in 2d Semiconductors—Considerations for Device Applications. *Adv. Funct. Mater.* **2020**, *30*, 1903929.

(12) Chen, X.-K.; Zeng, Y.-J.; Chen, K.-Q. Thermal Transport in Two-Dimensional Heterostructures. *Front. Mater.* **2020**, *7*, No. 578791.

(13) Allain, A.; Kang, J.; Banerjee, K.; Kis, A. Electrical Contacts to Two-Dimensional Semiconductors. *Nat. Mater.* **2015**, *14*, 1195−1205.

(14) Zhou, W.-X.; Chen, K.-Q. First-Principles Determination of Ultralow Thermal Conductivity of Monolayer Wse2. *Sci. Rep.* **2015**, *5*, 15070.

(15) Choi, Y.-G.; Jeong, D.-G.; Ju, H. I.; Roh, C. J.; Kim, G.; Mun, B. S.; Kim, T. Y.; Kim, S.-W.; Lee, J. S. Covalent-Bonding-Induced Strong Phonon Scattering in the Atomically Thin Wse2 Layer. *Sci. Rep.* **2019**, *9*, 7612.

(16) Lee, M.-J.; Ahn, J.-H.; Sung, J. H.; Heo, H.; Jeon, S. G.; Lee, W.; Song, J. Y.; Hong, K.-H.; Choi, B.; Lee, S.-H.; et al. Thermoelectric Materials by Using Two-Dimensional Materials with Negative Correlation between Electrical and Thermal Conductivity. *Nat. Commun.* **2016**, *7*, 12011.

(17) Yue, Y.; Zhang, J.; Tang, X.; Xu, S.; Wang, X. Thermal Transport across Atomic-Layer Material Interfaces. *Nanotechnol. Rev.* **2015**, *4*, 533−555.

(18) Yan, Z.; Chen, L.; Yoon, M.; Kumar, S. The Role of Interfacial Electronic Properties on Phonon Transport in Two-Dimensional Mos2 on Metal Substrates. *ACS Appl. Mater. Interfaces* **2016**, *8*, 33299−33306.

(19) Majumdar, A.; Reddy, P. Role of Electron−Phonon Coupling in Thermal Conductance of Metal−Nonmetal Interfaces. *Appl. Phys. Lett.* **2004**, *84*, 4768−4770.

(20) Lee, E.; Zhang, T.; Yoo, T.; Guo, Z.; Luo, T. Nanostructures Significantly Enhance Thermal Transport across Solid Interfaces. *ACS Appl. Mater. Interfaces* **2016**, *8*, 35505−35512.

(21) Hopkins, P. E.; Phinney, L. M.; Serrano, J. R.; Beechem, T. E. Effects of Surface Roughness and Oxide Layer on the Thermal Boundary Conductance at Aluminum/Silicon Interfaces. *Phys. Rev. B* **2010**, *82*, No. 085307.

(22) Hopkins, P. E. Thermal Transport across Solid Interfaces with Nanoscale Imperfections: Effects of Roughness, Disorder, Dislocations, and Bonding on Thermal Boundary Conductance. *Int. Scholarly Res. Not.* **2013**, *2013*, No. 682586.

(23) Hofmann, P.; Sklyadneva, I. Y.; Rienks, E. D. L.; Chulkov, E. V. Electron−Phonon Coupling at Surfaces and Interfaces. *New J. Phys.* **2009**, *11*, No. 125005.

(24) Wang, Y.; Lu, Z.; Roy, A. K.; Ruan, X. Effect of Interlayer on Interfacial Thermal Transport and Hot Electron Cooling in Metal-Dielectric Systems: An Electron-Phonon Coupling Perspective. *J. Appl. Phys.* **2016**, *119*, No. 065103.

(25) Giri, A.; Gaskins, J. T.; Donovan, B. F.; Szwejkowski, C.; Warzoha, R. J.; Rodriguez, M. A.; Ihlefeld, J.; Hopkins, P. E. Mechanisms of Nonequilibrium Electron-Phonon Coupling and Thermal Conductance at Interfaces. *J. Appl. Phys.* **2015**, *117*, 105105.

(26) Anisimov, S. I.; Kapeliovich, B. L.; Perel'Man, T. L. Electron Emission from Metal Surfaces Exposed to Ultrashort Laser Pulses. *Zh. Eksp. Teor. Fiz.* **1974**, *39*, 375−377.
(27) Qiu, T. Q.; Tien, C. L. Heat Transfer Mechanisms During Short-Pulse Laser Heating of Metals. *J. Heat Transfer* **1993**, *115*, 835−841.
(28) Mueller, B. Y.; Rethfeld, B. Relaxation Dynamics in Laser-Excited Metals under Nonequilibrium Conditions. *Phys. Rev. B* **2013**, *87*, No. 035139.
(29) Singh, N. Two-Temperature Model of Nonequilibrium Electron Relaxation: A Review. *Int. J. Mod. Phys. B* **2010**, *24*, 1141−1158.
(30) Hopkins, P. E.; Phinney, L. M.; Serrano, J. R. Re-Examining Electron-Fermi Relaxation in Gold Films with a Nonlinear Thermoreflectance Model. *J. Heat Transfer* **2011**, *133*, No. 044505.
(31) Gundrum, B. C.; Cahill, D. G.; Averback, R. S. Thermal Conductance of Metal-Metal Interfaces. *Phys. Rev. B* **2005**, *72*, No. 245426.
(32) Freedy, K. M.; Olson, D. H.; Hopkins, P. E.; McDonnell, S. J. Titanium Contacts to Mos2 with Interfacial Oxide: Interface Chemistry and Thermal Transport. *Phys. Rev. Mater.* **2019**, *3*, No. 104001.
(33) Vaziri, S.; Yalon, E.; Rojo, M. M.; Suryavanshi, S. V.; Zhang, H.; McClellan, C. J.; Bailey, C. S.; Smithe, K. K. H.; Gabourie, A. J.; Chen, V.; et al. Ultrahigh Thermal Isolation across Heterogeneously Layered Two-Dimensional Materials. *Sci. Adv.* **2019**, *5*, No. eaax1325.
(34) Rosul, M. G.; Lee, D.; Olson, D. H.; Liu, N.; Wang, X.; Hopkins, P. E.; Lee, K.; Zebarjadi, M. Thermionic Transport across Gold-Graphene-Wse₂ Van Der Waals Heterostructures. *Sci. Adv.* **2019**, *5*, No. eaax7827.
(35) Zhou, X.; Jankowska, J.; Li, L.; Giri, A.; Hopkins, P. E.; Prezhdo, O. V. Strong Influence of Ti Adhesion Layer on Electron−Phonon Relaxation in Thin Gold Films: Ab Initio Nonadiabatic Molecular Dynamics. *ACS Appl. Mater. Interfaces* **2017**, *9*, 43343−43351.
(36) Lu, T.-F.; Wang, Y.-S.; Tomko, J. A.; Hopkins, P. E.; Zhang, H.-X.; Prezhdo, O. V. Control of Charge Carrier Dynamics in Plasmonic Au Films by Tiox Substrate Stoichiometry. *J. Phys. Chem. Lett.* **2020**, *11*, 1419−1427.
(37) Zhou, X.; Tokina, M. V.; Tomko, J. A.; Braun, J. L.; Hopkins, P. E.; Prezhdo, O. V. Thin Ti Adhesion Layer Breaks Bottleneck to Hot Hole Relaxation in Au Films. *J. Chem. Phys.* **2019**, *150*, 184701.
(38) Wang, Y.-S.; Zhou, X.; Tomko, J. A.; Giri, A.; Hopkins, P. E.; Prezhdo, O. V. Electron−Phonon Relaxation at Au/Ti Interfaces Is Robust to Alloying: Ab Initio Nonadiabatic Molecular Dynamics. *J. Phys. Chem. C* **2019**, *123*, 22842−22850.
(39) Islam, M. R.; Kang, N.; Bhanu, U.; Paudel, H. P.; Erementchouk, M.; Tetard, L.; Leuenberger, M. N.; Khondaker, S. I. Tuning the Electrical Property Via Defect Engineering of Single Layer Mos2 by Oxygen Plasma. *Nanoscale* **2014**, *6*, 10033−10039.
(40) Kaushik, N.; Karmakar, D.; Nipane, A.; Karande, S.; Lodha, S. Interfacial N-Doping Using an Ultrathin Tio2 Layer for Contact Resistance Reduction in Mos2. *ACS Appl. Mater. Interfaces* **2016**, *8*, 256−263.
(41) Chen, J.-R.; Odenthal, P. M.; Swartz, A. G.; Floyd, G. C.; Wen, H.; Luo, K. Y.; Kawakami, R. K. Control of Schottky Barriers in Single Layer Mos2 Transistors with Ferromagnetic Contacts. *Nano Lett.* **2013**, *13*, 3106−3110.
(42) McDonnell, S.; Smyth, C.; Hinkle, C. L.; Wallace, R. M. Mos2−Titanium Contact Interface Reactions. *ACS Appl. Mater. Interfaces* **2016**, *8*, 8289−8294.
(43) Duda, J. C.; Yang, C.-Y. P.; Foley, B. M.; Cheaito, R.; Medlin, D. L.; Jones, R. E.; Hopkins, P. E. Influence of Interfacial Properties on Thermal Transport at Gold:Silicon Contacts. *Appl. Phys. Lett.* **2013**, *102*, 081902.
(44) Mao, R.; Kong, B. D.; Kim, K. W. Thermal Transport Properties of Metal/Mos2 Interfaces from First Principles. *J. Appl. Phys.* **2014**, *116*, No. 034302.
(45) Freedy, K. M.; Zhu, T.; Olson, D. H.; Litwin, P. M.; Hopkins, P. E.; Zebarjadi, M.; McDonnell, S. J. Interface Chemistry and Thermoelectric Characterization of Ti and Tiox Contacts to Mbe-Grown Wse2. *2D Mater.* **2020**, *7*, No. 045033.
(46) Prezhdo, O. V. Modeling Non-Adiabatic Dynamics in Nanoscale and Condensed Matter Systems. *Acc. Chem. Res.* **2021**, *54*, 4239−4249.
(47) Runge, E.; Gross, E. K. U. Density-Functional Theory for Time-Dependent Systems. *Phys. Rev. Lett.* **1984**, *52*, 997−1000.
(48) Tully, J. C. Molecular Dynamics with Electronic Transitions. *J. Chem. Phys.* **1990**, *93*, 1061−1071.
(49) Wang, L.; Akimov, A.; Prezhdo, O. V. Recent Progress in Surface Hopping: 2011−2015. *J. Phys. Chem. Lett.* **2016**, *7*, 2100−2112.
(50) Akimov, A. V.; Prezhdo, O. V. The Pyxaid Program for Non-Adiabatic Molecular Dynamics in Condensed Matter Systems. *J. Chem. Theory Comput.* **2013**, *9*, 4959−4972.
(51) Akimov, A. V.; Prezhdo, O. V. Advanced Capabilities of the Pyxaid Program: Integration Schemes, Decoherence Effects, Multi-excitonic States, and Field-Matter Interaction. *J. Chem. Theory Comput.* **2014**, *10*, 789−804.
(52) Agrawal, S.; Lin, W.; Prezhdo, O. V.; Trivedi, D. J. Ab Initio Quantum Dynamics of Charge Carriers in Graphitic Carbon Nitride Nanosheets. *J. Chem. Phys.* **2020**, *153*, No. 054701.
(53) Akimov, A. V.; Asahi, R.; Jinnouchi, R.; Prezhdo, O. V. What Makes the Photocatalytic Co2 Reduction on N-Doped Ta2o5 Efficient: Insights from Nonadiabatic Molecular Dynamics. *J. Am. Chem. Soc.* **2015**, *137*, 11517−11525.
(54) Li, L.; Long, R.; Bertolini, T.; Prezhdo, O. V. Sulfur Adatom and Vacancy Accelerate Charge Recombination in Mos2 but by Different Mechanisms: Time-Domain Ab Initio Analysis. *Nano Lett.* **2017**, *17*, 7962−7967.
(55) Gumber, S.; Agrawal, S.; Prezhdo, O. V. Excited State Dynamics in Dual-Defects Modified Graphitic Carbon Nitride. *J. Phys. Chem. Lett.* **2022**, *13*, 1033−1041.
(56) Shi, R.; Vasenko, A. S.; Long, R.; Prezhdo, O. V. Edge Influence on Charge Carrier Localization and Lifetime in Ch3nh3pbbr3 Perovskite: Ab Initio Quantum Dynamics Simulation. *J. Phys. Chem. Lett.* **2020**, *11*, 9100−9109.
(57) Wu, Y. F.; Chu, W. B.; Vasenko, A. S.; Prezhdo, O. V. Common Defects Accelerate Charge Carrier Recombination in Cssni3 without Creating Mid-Gap States. *J. Phys. Chem. Lett.* **2021**, *12*, 8699−8705.
(58) Cheng, C.; Zhu, Y. H.; Fang, W. H.; Long, R.; Prezhdo, O. V. Co Adsorbate Promotes Polaron Photoactivity on the Reduced Rutile Tio2(110) Surface. *JACS Au* **2022**, *2*, 234−245.
(59) Zhu, Y. H.; Fang, W. H.; Rubio, A.; Long, R.; Prezhdo, O. V. The Twist Angle Has Weak Influence on Charge Separation and Strong Influence on Recombination in the Mos2/Ws2 Bilayer: Ab Initio Quantum Dynamics. *J. Mater. Chem. A* **2022**, *10*, 8324−8333.
(60) Shi, R.; Fang, Q.; Vasenko, A. S.; Long, R.; Fang, W.-H.; Prezhdo, O. V. Structural Disorder in Higher-Temperature Phases Increases Charge Carrier Lifetimes in Metal Halide Perovskites. *J. Am. Chem. Soc.* **2022**, *144*, 19137−19149.
(61) Kresse, G.; Hafner, J. Ab Initio Molecular Dynamics for Liquid Metals. *Phys. Rev. B* **1993**, *47*, 558−561.
(62) Perdew, J. P.; Burke, K.; Ernzerhof, M. Generalized Gradient Approximation Made Simple. *Phys. Rev. Lett.* **1996**, *77*, 3865−3868.
(63) Kresse, G.; Joubert, D. From Ultrasoft Pseudopotentials to the Projector Augmented-Wave Method. *Phys. Rev. B* **1999**, *59*, 1758−1775.
(64) Grimme, S.; Antony, J.; Ehrlich, S.; Krieg, H. A Consistent and Accurate Ab Initio Parametrization of Density Functional Dispersion Correction (Dft-D) for the 94 Elements H-Pu. *J. Chem. Phys.* **2010**, *132*, 154104.
(65) Reckien, W.; Janetzko, F.; Peintinger, M. F.; Bredow, T. Implementation of Empirical Dispersion Corrections to Density Functional Theory for Periodic Systems. *J. Comput. Chem.* **2012**, *33*, 2023−2031.

(66) Zhang, H.; Zhu, J.; Zhang, H.; Zhang, J.; Zhang, Y.; Lu, Z.-H. The Structural, Electronic and Catalytic Properties of Aun (N = 1−4) Nanoclusters on Monolayer Mos2. *RSC Adv.* **2017**, *7*, 42529−42540.
(67) Momma, K.; Izumi, F. Vesta 3 for Three-Dimensional Visualization of Crystal, Volumetric and Morphology Data. *J. Appl. Crystallogr.* **2011**, *44*, 1272−1276.
(68) Chu, W. B.; Zheng, Q. J.; Akimov, A. V.; Zhao, J.; Saidi, W. A.; Prezhdo, O. V. Accurate Computation of Nonadiabatic Coupling with Projector Augmented-Wave Pseudopotentials. *J. Phys. Chem. Lett.* **2020**, *11*, 10073−10080.
(69) Chu, W. B.; Prezhdo, O. V. Concentric Approximation for Fast and Accurate Numerical Evaluation of Nonadiabatic Coupling with Projector Augmented-Wave Pseudopotentials. *J. Phys. Chem. Lett.* **2021**, *12*, 3082−3089.
(70) Zhao, P.; Liu, D. S.; Chen, G. Energy Alignment Induced Large Rectifying Behavior in Endoheral Fullerene Dimers. *J. Chem. Phys.* **2013**, *139*, 084318.
(71) An, Y. P.; Zhang, M. J.; Wang, T. X.; Wang, G. T.; Fu, Z. M. Rectifications in Organic Single-Molecule Diodes Alkanethiolate-Terminated Heterocyclics. *Phys. Lett. A* **2016**, *380*, 923−926.
(72) Zhang, Y. S.; Guo, Y. Spin and Valley Dependent Line-Type Resonant Peaks in Electrically and Magnetically Modulated Silicene Quantum Structures. *Eur. Phys. J. B* **2017**, *90*, 27.
(73) Rasmussen, F. A.; Thygesen, K. S. Computational 2d Materials Database: Electronic Structure of Transition-Metal Dichalcogenides and Oxides. *J. Phys. Chem. C* **2015**, *119*, 13169−13183.
(74) Prezhdo, O. V.; Rossky, P. J. Evaluation of Quantum Transition Rates from Quantum-Classical Molecular Dynamics Simulations. *J. Chem. Phys.* **1997**, *107*, 5863−5878.
(75) Li, W.; She, Y. L.; Vasenko, A. S.; Prezhdo, O. V. Ab Initio Nonadiabatic Molecular Dynamics of Charge Carriers in Metal Halide Perovskites. *Nanoscale* **2021**, *13*, 10239−10265.
(76) Avanesian, T.; Christopher, P. Adsorbate Specificity in Hot Electron Driven Photochemistry on Catalytic Metal Surfaces. *J. Phys. Chem. C* **2014**, *118*, 28017−28031.

https://doi.org/10.1021/acsami.2c18793
ACS Appl. Mater. Interfaces 2022, 14, 57197−57205